An unconventional method for measuring the Tc L_3-edge of technetium compounds

Peter E. R. Blanchard,[a] Emily Reynolds,[a] Brendan J. Kennedy,[a]* Chris D. Ling,[a] Zhaoming Zhang,[b] Gordon Thorogood,[b] Bruce C. C. Cowie[c] and Lars Thomsen[c]

[a]School of Chemistry, The University of Sydney, Sydney, NSW 2006, Australia, [b]Australian Nuclear Science and Technology Organisation, Lucas Heights, NSW 2234, Australia, and [c]Australian Synchrotron, 800 Blackburn Road, Clayton, Victoria 3168, Australia.
*E-mail: brendan.kennedy@sydney.edu.au

Tc L_3-edge XANES spectra have been collected on powder samples of $SrTcO_3$ (octahedral Tc^{4+}) and NH_4TcO_4 (tetrahedral Tc^{7+}) immobilized in an epoxy resin. Features in the Tc L_3-edge XANES spectra are compared with the pre-edge feature of the Tc K-edge as well as other $4d$ transition metal L_3-edges. Evidence of crystal field splitting is obvious in the Tc L_3-edge, which is sensitive to the coordination number and oxidation state of the Tc cation. The Tc L_3 absorption edge energy difference between $SrTcO_3$ (Tc^{4+}) and NH_4TcO_4 (Tc^{7+}) shows that the energy shift at the Tc L_3-edge is an effective tool for studying changes in the oxidation states of technetium compounds. The Tc L_3-edge spectra are compared with those obtained from Mo and Ru oxide standards with various oxidation states and coordination environments. Most importantly, fitting the Tc L_3-edge to component peaks can provide direct evidence of crystal field splitting that cannot be obtained from the Tc K-edge.

1. Introduction

The $4d$ transition metal oxides continue to be one of the most exciting areas of solid-state chemistry, exhibiting a wide range of interesting magnetic and electronic properties. Of the $4d$ transition metal oxides, the structural and electronic properties of technetium oxides have remained somewhat elusive. This is not surprising given the absence of stable technetium isotopes and the radioactivity of the existing isotopes (Deutsch et al., 1983). One isotope in particular, ^{99}Tc, is a common byproduct in nuclear fission that decays by β-emission with a relatively long half-life of 2.12×10^5 years. As such, there has been considerable effort to develop solid-state forms (e.g. pyrochlores) of technetium in order to sequester technetium from nuclear waste (Hartmann et al., 2011, 2012). Technetium ($5s^2 4d^5$) is known to adopt a wide range of oxidation states analogous to manganese ($4s^2 3d^5$) and rhenium ($6s^2 5d^5$) (Kotegov et al., 1968). Technetium oxides are also known to exhibit magnetic properties that are unusual for $4d$ and $5d$ transition metal oxides (Rodriguez et al., 2011; Avdeev et al., 2011). Recently the perovskites $CaTcO_3$ and $SrTcO_3$, which adopt an orthorhombic structure in space group $Pnma$, were shown to exhibit antiferromagnetic ordering with exceptionally high Néel temperatures of 800 and 1023 K, respectively (Rodriguez et al., 2011; Avdeev et al., 2011). The magnetic moment on the Tc^{4+} cations in $SrTcO_3$

was relatively unaffected by a high-temperature orthorhombic cubic phase transition at 800 K (Thorogood et al., 2011a). It has been suggested that the unusual magnetic ordering in these materials originates from the half-filling of the t_{2g} band (Avdeev et al., 2011; Middey et al., 2012; Mravlje et al., 2012).

Because of the radioactive nature of technetium, there are relatively few tools available for analyzing the electronic properties of these materials compared with the other $4d$ transition metals. Tc K-edge X-ray absorption near-edge structure (XANES) has proven to be an effect tool for studying the oxidation state and coordination environment of Tc (Antonini et al., 1983; Almahamid et al., 1995; Mausolf et al., 2011; Poineau et al., 2008; Ferrier et al., 2012; Thorogood et al., 2011b). However, the Tc K-edge XANES spectrum, which predominantly corresponds to the dipole transition of $1s$ electrons into empty $5p$ states, is limited by a broad line shape and can only provide indirect information on the Tc $4d$ bonding states via the unoccupied p component in p–d hybridized orbitals. We have previously shown that the L_3-edge, which corresponds to the transition of $2p_{3/2}$ electrons into unoccupied $4d$ states, is a sensitive probe for directly analyzing the bonding states of $4d$ transition metal oxide with empty or partially filled d orbitals (Zhou et al., 2009; Ting et al., 2010; Ricciardo et al., 2010; Qasim et al., 2011; Blanchard et al., 2012; Reynolds et al., 2013). In these studies, we demonstrated that crystal field splitting can be extracted from the $4d$ tran-

sition metal L_3-edge by fitting the spectra to component peaks (it is difficult to extract the crystal-field-splitting energy from the K-edge since the K-edge spectra do not directly probe the metal $4d$ states). To our knowledge, the Tc L-edge has never been measured. This is likely to be due to the radioactive nature of technetium (limiting the amount and form of technetium that can be analyzed at a synchrotron facility) and the inherent safety difficulties in conducting a Tc L-edge XANES experiment (the relatively weak excitation energy of the Tc L-edge at $\sim$2680 eV means that samples would have to be directly exposed to the incoming X-ray beam without any shielding).

Herein, we report on a method for measuring the Tc L_3-edge of technetium oxides that involves immobilizing powder samples in an epoxy resin. Although immobilizing samples in epoxy is a common practice in electron microscopy, it usually involves a much larger quantity than the allowed milligram quantity for Tc-containing samples. Furthermore, immobilizing powder samples in an epoxy resin is not common practice in soft X-ray experiments due to the relatively short penetration depth of soft X-rays compared with hard X-rays. It has previously been demonstrated that soft X-ray absorption spectroscopy experiments can be conducted on actinides (uranium- and thorium-based chlorides) by embedding the powder in a polystyrene matrix (Kozimor *et al.*, 2009); in that work, the compounds of interest and the polystyrene were dissolved in a volatile solvent and the solid formed by evaporation of the solution. Since it is not possible to dissolve many condensed materials such as $SrTcO_3$, an alternative approach has been employed to study the Tc L_3-edge of $SrTcO_3$ (Tc^{4+}) and NH_4TcO_4 (Tc^{7+}) using an epoxy resin to immobilize the samples rather than polystyrene. We will demonstrate that both fluorescence (FLY) and total electron (TEY) yield measurements can be collected using this sample preparation method. These spectra will be compared with their respective Tc K-edge XANES spectra as well as the L_3-edge of other $4d$ transition metal oxides, specifically the neighboring Mo and Ru. The goals of this work are, firstly, to determine if spectra collected from epoxy-embedded samples are in fact representative of the bulk material and, secondly, to establish if information on the electronic and local structure of Tc cations can be obtained from the Tc L_3-edge XANES spectra.

2. Experimental

Caution! ^{99}Tc is a β^- emitter (E_{max} = 0.29 MeV). Appropriate shielding was employed during the synthesis and all manipulations. The purity of all starting materials was greater than 99%. NH_4TcO_4 was obtained from Oak Ridge National Laboratory and used as received. Although the sample was black in color, X-ray diffraction measurements indicated the sample to be phase pure. Polycrystalline samples of $SrTcO_3$ were synthesized using solid-state methods described elsewhere (Thorogood *et al.*, 2011a). Stoichiometric amounts of NH_4TcO_4 and $Sr(NO_3)_2$ were dry rolled in polyethylene vials for 16 h, to ensure complete mixing, and annealed at 973 K
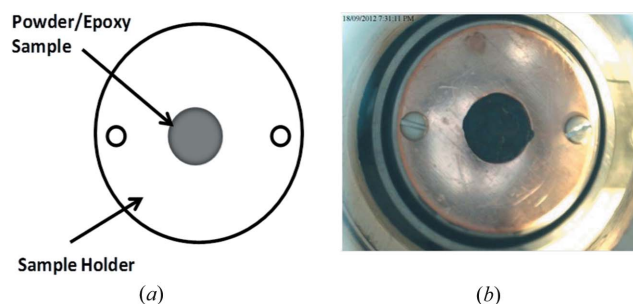
Figure 1
(*a*) Diagram of a powder sample embedded in an epoxy resin mounted onto a sample stage and (*b*) an image of the $CaRuO_3$ sample used in the experiment. The diameter of the epoxy disc is approximately 1.1 mm.

under Ar for 1 h. The samples were re-ground, wet ball-milled in cyclohexane for 16 h, air-dried, pressed into pellets and annealed under Ar at 1423 K for 4 h. The purity of the samples was confirmed by powder X-ray diffraction (see supporting information[1]).

All L_3-edge XANES spectra were collected on the soft X-ray beamline at the Australian Synchrotron (Cowie *et al.*, 2010). In order to comply with the Australian Radiation Protection and Nuclear Safety Agency regulations, the amount of technetium used in these measurements was limited to $\sim$5 mg per sample. Technetium-containing powder samples were mixed with a minimum amount of industrial epoxy resin forming an extremely thick paste. The mixture was left to harden overnight by which time the technetium compounds were effectively immobilized. Swipe tests of the immobilized samples gave (beta) values of less than 100 counts s^{-1} A similar method was used to prepare epoxy-embedded $CaRuO_3$ (Fig. 1). Ru and Mo oxide standards were lightly dusted onto double-sided carbon tape (SPI Supplies).

All samples were inserted into the vacuum chamber *via* a load lock. The pressure inside the analysis chamber was maintained at $<10^{-9}$ mbar during the measurements. The epoxy encapsulated samples did not significantly degas. Spectra were collected from $\sim$30 eV below to $\sim$80 eV above the edge, with a step size of 0.2 eV using both TEY and FLY modes (except that the FLY signal at the Ru L_3-edge had to be collected from another beamline, see §3). All spectra were recorded simultaneously with the TEY signal measured from Mo (Mo and Tc L_3-edge) or $Ru(OH)Cl_3$ (Ru L_3-edge) reference samples positioned upstream in the beamline. The reference sample removed approximately 10% of the beam intensity. Mo L_3-edge spectra were calibrated to the Mo L_3-edge of Mo foil, with the maximum of the first derivate set to 2520 eV. Tc L_3-edge spectra were calibrated to the Mo L_2-edge of Mo foil, with the maximum of the first derivate set to 2625 eV. Due to the relatively weak edge jump, the Ru L_3-edge spectra were calibrated against the maximum peak height of the Ru L_3-edge XANES spectra of $Ru(OH)Cl_3$ rather than the maximum of the first derivative. The maximum peak height of the Ru L_3-edge XANES spectra of $Ru(OH)Cl_3$

---

[1] Supporting information for this paper is available from the IUCr electronic archives (Reference: HF5261).

was at 2840.1 eV, based on the calibration against Ru metal with the maximum of the first derivate set to 2838 eV.

Tc K-edge XANES spectra of $SrTcO_3$ and NH_4TcO_4 were collected in transmission mode on the X-ray absorption spectroscopy beamline at the Australian Synchrotron (Glover *et al.*, 2007). Powder samples were mixed with an appropriate amount of BN, sandwiched between two Kapton tapes and positioned directly in front of the X-ray beam. Spectra were collected from ∼200 eV below to ∼1000 eV above the edge with a step size of 0.25 eV around the edge and a dwell time of 1 s. X-rays were monochromated using an Si(111) monochromator, which was detuned by 50% to reject higher harmonics. The Tc K-edge was calibrated against Mo foil with the maximum of the first derivative of the Mo K-edge set to 20000 eV.

All absorption-edge energies are reported from the maximum of the first derivative of their respective edges. All XANES data were analyzed using the *Athena* and *CasaXPS* software packages (Ravel & Newville, 2005; Fairley, 2012).

3. Results and discussion

Measurement of the Tc L-edge spectra utilized the ultra-high-vacuum soft X-ray beamline at the Australian Synchrotron. The essential safety requirements for the measurements were (i) the sample was encapsulated in such a way that no loose material could be inadvertently introduced into the beamline and (ii) the amount of radioactive material was within the regulated limits of a general user beamline. For high-energy X-ray experiments, X-ray transparent windows can be employed to contain the sample; however, these are unsuitable for low-energy soft X-ray measurements. Our strategy was to form a solid pellet of the technetium compound using an epoxy host. Before measuring the Tc L_3-edge, a proof-of-concept experiment was conducted to ensure that this sample preparation technique produces quality XANES spectra representative of the bulk material. For this, the Ru L_3-edge XANES spectrum of $CaRuO_3$ was collected. This was chosen because its absorption-edge energy is greater than that of the Tc L_3-edge and is near the upper limit of the energy range of the soft X-ray spectroscopy beamline (Cowie *et al.*, 2010). Consequently, the X-ray signal at the Ru L_3-edge would be much weaker than that at the Tc L_3-edge.

The Ru L_3-edge XANES spectra of $CaRuO_3$, measured both as a powder dusted on carbon tape and as an epoxy-embedded sample, are shown in Fig. 2. Overall, the Ru L_3-edge spectra shown here are similar to those previously reported for $CaRuO_3$ (Zhou *et al.*, 2009; Wu *et al.*, 2003; Bréard *et al.*, 2007). The Ru L_3-edge XANES spectrum of $CaRuO_3$, where Ru occupies the slightly distorted octahedral site, consists of two features that correspond to the transition of a $2p_{3/2}$ electron into the unoccupied $4d$–t_{2g} (lower energy peak) and $4d$–e_g (higher energy peak) states. Such features are typically observed in $4d$ transition metal L-edge XANES spectra (Ting *et al.*, 2010; Qasim *et al.*, 2011; Blanchard *et al.*, 2012; Reynolds *et al.*, 2013; Blanchard *et al.*, 2013a). The peak corresponding to transitions to the t_{2g} states appears as a lower
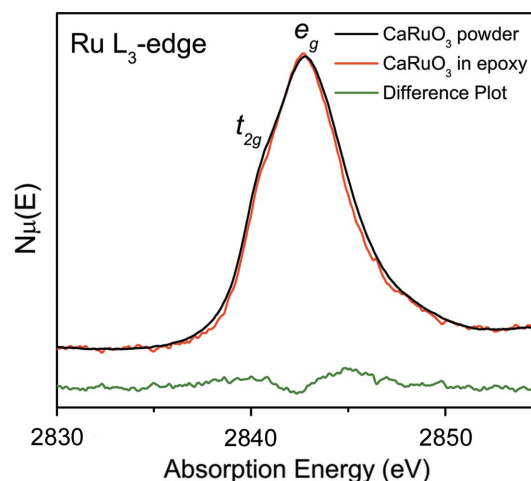
Figure 2
Ru L_3-edge XANES spectra of powder (black line) and epoxy-embedded (red line) $CaRuO_3$. The difference plot (green line) shows that the spectra are essentially identical. Both spectra were collected in TEY mode.

energy shoulder due to the partial occupancy of the t_{2g} states in Ru^{4+} ($t_{2g}{}^4 e_g{}^0$). As shown in Fig. 2, the Ru L_3-edge spectrum of the powder form of $CaRuO_3$ is nearly identical to that of the epoxy-embedded form. The crystal field splitting, estimated from fitting the Ru L_3-edge to component peaks corresponding to the t_{2g} and e_g peaks, was estimated to be ∼3.0 eV for both samples (more details later in the paper). Both spectra are similar to the FLY Ru L_3-edge spectrum of $CaRuO_3$ collected at the National Synchrotron Radiation Research Center in Hsinchu, Taiwan (see supporting information), confirming that the TEY signal is representative of the bulk material and that XANES spectra can be obtained using this sample preparation technique. We were unable to collect the FLY spectra on the soft X-ray spectroscopy beamline at the Australian Synchrotron because the Ru L_3-edge is outside the designed range of the FLY detector.

Our preliminary experiment with $CaRuO_3$ suggests that embedding powder samples in an epoxy resin is a feasible method for measuring the Tc L_3-edge. Consequently, we collected the Tc L_3-edge spectra from ∼5 mg $SrTcO_3$ and NH_4TcO_4 samples embedded in epoxy, and compared them with their respective K-edge XANES spectra (Fig. 3). Absorption-edge energies are tabulated in Table 1. Both Tc L_3-edges presented in Fig. 3 were collected in TEY mode. As shown in Fig. 4, the FLY signal is considerably weaker than the TEY signal. The FLY signal has a similar line shape to the TEY signal, confirming that the TEY signal of the Tc L_3-edge is representative of the bulk material and suitable for this analysis. The K and L edges have advantages and disadvantages when it comes to characterizing the electronic and structural properties of Tc oxides. Analysis of the Tc K-edge absorption-edge energy is particularly useful in identifying Tc^{4+} and Tc^{7+} species (Mausolf *et al.*, 2011; Ferrier *et al.*, 2012). The Tc L_3-edge absorption-edge energy of $SrTcO_3$ (2677.0 eV) is less than that of NH_4TcO_4 (2678.5 eV), but the difference between them (1.5 eV) is much less than the difference of 4.5 eV observed at the Tc K-edge ($SrTcO_3$,

Peter E. R. Blanchard *et al.* • An unconventional method for measuring the Tc L_3-edge

Table 1
Absorption-edge energies for the various $4d$ transition metal oxides.

Sample	Oxidation state	Coordination number	Electronic configuration	Absorption edge	Absorption edge energy (eV)
(NH$_4$)TcO$_4$	Tc^{7+}	4	[Kr] $4d^0$	Tc L_3-edge	2678.5
				Tc K-edge	21062.7
SrTcO$_3$	Tc^{4+}	6	[Kr] $4d^3$	Tc L_3-edge	2677.0
				Tc K-edge	21058.2
Bi$_2$MoO$_6$ (LT)	Mo^{6+}	6	[Kr] $4d^0$	Mo L_3-edge	2523.0
Bi$_2$MoO$_6$ (HT)	Mo^{6+}	4	[Kr] $4d^0$	Mo L_3-edge	2523.0
MoO$_2$	Mo^{4+}	6	[Kr] $4d^2$	Mo L_3-edge	2521.4
Sr$_2$RuYO$_6$	Ru^{5+}	6	[Kr] $4d^3$	Ru L_3-edge	2839.1
SrRuO$_3$	Ru^{4+}	6	[Kr] $4d^4$	Ru L_3-edge	2838.2
CaRuO$_3$	Ru^{4+}	6	[Kr] $4d^4$	Ru L_3-edge	2838.1

21058.2 eV; NH$_4$TcO$_4$, 21062.7 eV). Both energy shifts are consistent with the Tc cations in SrTcO$_3$ having the lower oxidation state.

The most striking feature of the Tc L_3-edge is the line shape. The Tc L_3-edge line shape of NH$_4$TcO$_4$ consists of two features (labeled A and B in Fig. 3a). As previously discussed, features in $4d$ transition metal L-edge spectra typically result

from the crystal field splitting of the $4d$ states. The Tc^{7+} cations have a tetrahedral coordination environment in NH$_4$TcO$_4$ and the features in the L_3-edge correspond to transitions to the empty e (feature A) and t_2 (feature B) states. Similar features corresponding to transitions to the partially occupied t_{2g} and e_g states are observed in SrTcO$_3$ with the e_g states undergoing further splitting due to distortion of the TcO$_6$ octahedra. This will be discussed further below. Evidence of crystal field splitting is not obvious in the Tc K-edge spectra, which is expected as the K-edge spectra do not probe the $4d$ states directly. Instead the Tc K-edge spectrum consists of a pre-edge feature which corresponds to the dipole forbidden transition of a $1s$ electron into $4d$ states via p–d hybridization (Kettle, 2008). In the Tc K-edge spectrum of NH$_4$TcO$_4$, the pre-edge contains an intense peak because the tetrahedral site occupied by the Tc^{7+} cation has T_d symmetry which allows the hybridization of metal $4d$ and $5p$ states (Kettle, 2008). In contrast, the Tc K-edge spectrum of SrTcO$_3$, where the Tc^{4+} cation occupies a nearly centrosymmetric octahedral site (O_h), does not contain an obvious pre-edge feature due to the lack of d–p hybridization (as there are no irreducible representations of O_h to which both p and d orbitals belong) (Kettle, 2008). A pre-edge feature at the K-edge can manifest in highly distorted octahedral systems because the reduced symmetry would allow a certain degree of p–d mixing (Yamamoto, 2008). Since the pre-edge feature results from a transition to the p component in d–p hybridized orbitals (not d-orbitals directly), it is difficult to extract information on crystal field splitting from $4d$ transition metal K-edge XANES spectra. The features at the Tc K-edge are also broader than those at the L-edge due to lifetime broadening. In general, the L-edge spectra appear to be more sensitive to changes in crystal field splitting, therefore having a greater sensitivity to changes in the local structure.

(a)

(b)
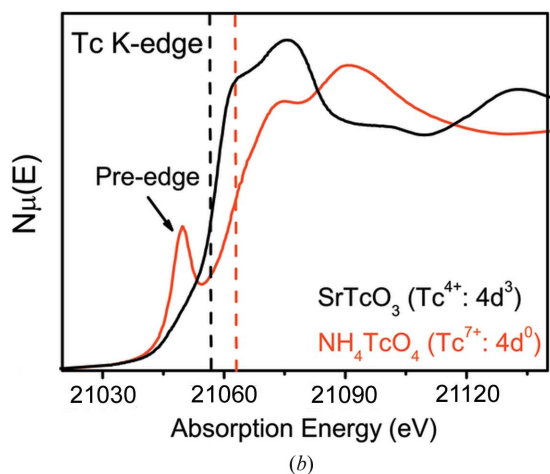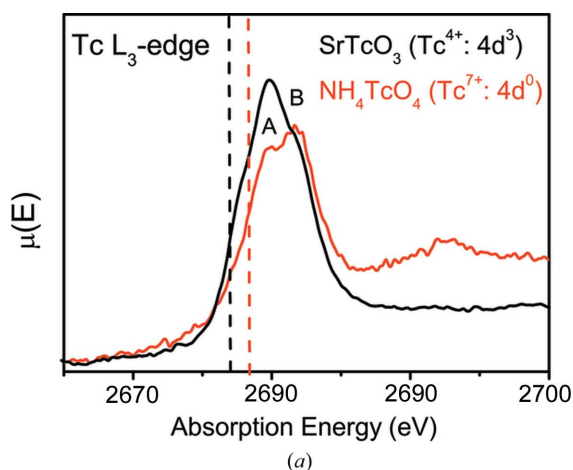
Figure 3
(a) Tc L_3-edge (collected in TEY mode) and (b) K-edge (collected in transmission mode) XANES spectra of SrTcO$_3$ (octahedral Tc^{4+}) and NH$_4$TcO$_4$ (tetrahedral Tc^{7+}). Dashed lines correspond to the absorption-edge energies of SrTcO$_3$ (black line) and NH$_4$TcO$_4$ (red line).
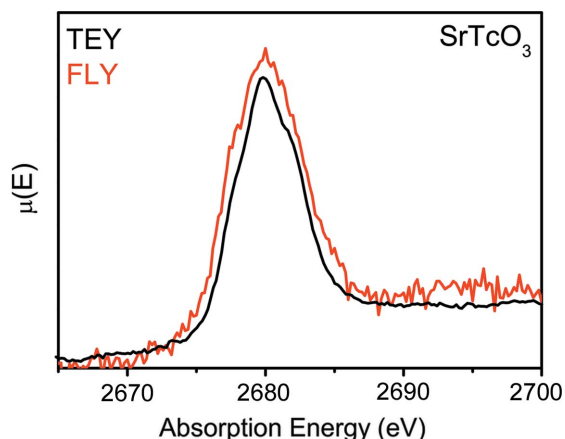
Figure 4
Tc L_3-edge XANES spectra of SrTcO$_3$ collected in TEY (black line) and FLY (red line) mode, respectively.

Since these appear to be the first measurements at the Tc L_3-edge, the experimental XANES spectra of $SrTcO_3$ (Tc^{4+}) and NH_4TcO_4 (Tc^{7+}) were compared with appropriate Mo and Ru L_3-edge standards (Fig. 5) measured on the same beamline. The difference in the Tc L_3-edge absorption edge energy between the Tc^{4+} and Tc^{7+} species (1.5 eV) is similar to that observed at the Mo L_3-edge between the Mo^{6+} and Mo^{4+} species (~1.6 eV; Veith *et al.*, 2005) and larger than that at the Ru L_3-edge between Ru^{4+} and Ru^{5+} oxides (0.9 eV). The energy shift in the Tc L_3-edge is somewhat smaller than expected for such a large change in oxidation state. Although there is no difference in the Mo L_3-edge absorption-edge energy of the high-temperature (tetrahedral Mo^{6+}) and low-temperature (octahedral Mo^{6+}) polymorphs of Bi_2MoO_6 (2523 eV), we cannot confirm from this study that the coordination environment of Tc has no effect on the Tc L_3-edge absorption-edge energy. Regardless, the Tc L_3-edge absorption-edge energy does appear to be sensitive to the oxidation state of Tc. The line shape of the Tc L_3-edge shares similarities to that of the Mo and Ru L_3-edge spectra. In general, features in XANES L_3-edge spectra of $4d^0$ transition metals correspond to the crystal field splitting of the $4d$ states. This is well illustrated by comparing the Mo L_3-edge spectra of the high-temperature and low-temperature polymorphs of Bi_2MoO_6

(Sankar *et al.*, 1995; Buttrey *et al.*, 1994; Laarif *et al.*, 1984). The Mo L_3-edge spectra of both forms of Bi_2MoO_6 consist of two features (labeled A and B in Fig. 5*a*), which correspond to transitions to the doubly degenerate e and triply degenerate t_2 states in tetrahedral systems, and to the triply degenerate t_{2g} and doubly degenerate e_g states in octahedral systems, respectively (Bare *et al.*, 1993; Hu *et al.*, 1995; Lede *et al.*, 2002). The difference in intensity of the two features reflects the reversal of the orbital energies and the appropriate degeneracy of these (3:2 in octahedral systems *versus* 2:3 in tetrahedral systems, under simplified crystal field theory). The Tc L_3-edge of NH_4TcO_4 has a similar line shape to the high-temperature form of Bi_2MoO_6, consistent with the presence of a tetrahedral $4d^0$ transition metal.

The line shape of the Tc L_3-edge spectrum of $SrTcO_3$ (Tc^{4+}) is similar to that of other octahedral $4d$ transition metals with partially occupied $4d$ states, such as MoO_2 (Mo^{4+} d^2) and $SrRuO_3$ (Ru^{4+} d^4). As mentioned earlier, the intensity of feature A is weaker than that of feature B due to partial filling of the t_{2g} state. The splitting between the t_{2g} and e_g orbitals depends on the ligand field strength, which typically increases as the oxidation state increases (with similar bond distances). The transition into the t_{2g} states appears as a discrete peak (labeled A in Fig. 5*b*) in the L_3-edge spectra of $Sr_2Ru^VYO_6$ but only as a low-energy shoulder in $Sr(Ca)Ru^{IV}O_3$ and $SrTc^{IV}O_3$, consistent with the higher Ru oxidation state in Sr_2RuYO_6. In octahedral systems, feature B, which corresponds to the e_g states, shows asymmetry towards higher energy. This asymmetry has been observed in the Zr L_3-edge of pyrochlores $Ln_2Zr_2O_7$ (Blanchard *et al.*, 2012), and is believed to be a consequence of the sensitivity of the e_g states to local distortions due to the overlap of d_{z^2} and $d_{x^2-y^2}$ states with ligand states. Such distortions can result in broadening and splitting of the e_g peak (Schneller *et al.*, 2008).

Further information on the local structure can be obtained by fitting the Tc L_3-edge to component peaks. Such analysis has previously been employed to study the local structure of zirconate and hafnate pyrochlores (Qasim *et al.*, 2011; Blanchard *et al.*, 2012, 2013*b*; Reynolds *et al.*, 2013). As shown in Fig. 6, the spectra were fitted to pseudo-Voigt peaks with an arctan background. Fitted spectra of the Ru and Mo L_3-edge XANES spectra can be found in the supporting information (Fig. S2 of the supporting information). Results of the fitting are presented in Table 2. In all compounds listed, feature A was fitted to a single component peak. The number of components required to fit feature B varied depending on the coordination environment. In compounds where the metal cation occupies a tetrahedral coordination environment, only one component peak was required to fit feature B. In compounds where the metal is six-coordinate, two component peaks (labeled B1 and B2) were required to fit feature B. This is likely to be due to localized distortions of the metal octahedra (Ray *et al.*, 2011; Ikeno *et al.*, 2013). The splitting of feature B into two peaks can be confirmed by analysing the first derivative XANES spectrum. For example, the first derivative Tc L_3-edge XANES spectrum of $SrTcO_3$ (see supporting information) has three peak maxima which
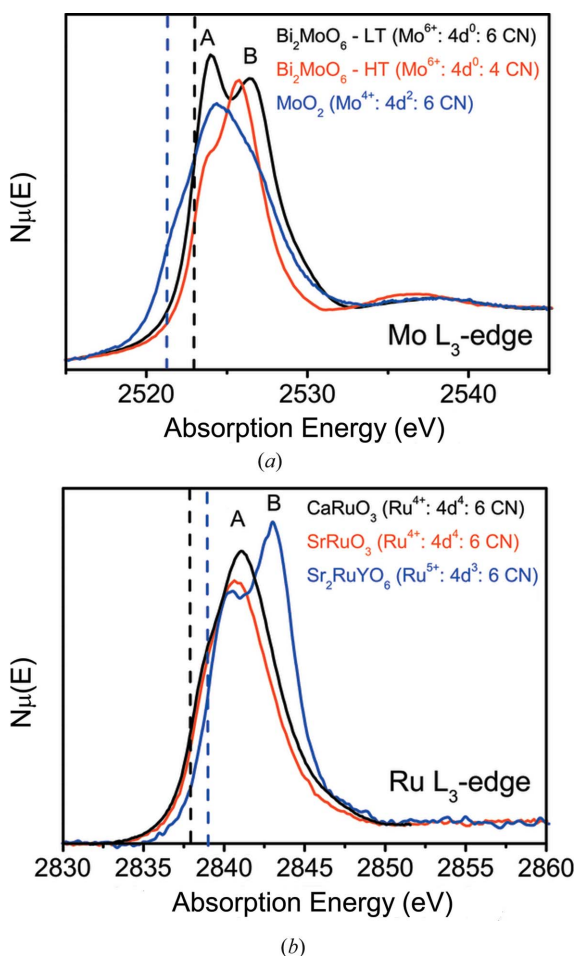
Figure 5
(*a*) Mo and (*b*) Ru L_3-edge XANES spectra of various Mo and Ru oxide standards. All spectra were collected in TEY mode.

Table 2
Fitting parameters to the 4*d* transition metal *L*₃-edges.

E_i is the energy of peak i and I_i is the intensity of peak i estimated from peak fitting. The width of the peaks and the estimated splitting between peaks A and B1 (ΔE) are also given.

Sample	E_A (eV)	E_{B1} (eV)	E_{B2} (eV)	I_A	I_{B1}	I_{B2}	Peak width	ΔE (eV)
(NH₄)TcO₄	2679.5	2682.0	N/A	2.682	3.201	N/A	2.7	2.5
SrTcO₃	2678.0	2680.0	2682.3	4.265	9.283	6.136	2.7	2.9
Bi₂MoO₆ (LT)	2524.0	2526.7	2529.0	10.534	9.37	2.19	2.5	3.1
Bi₂MoO₆ (HT)	2523.6	2525.9	N/A	3.766	11.377	N/A	2.4	2.0
MoO₂	2523.0	2525.0	2527.4	4.887	8.168	5.046	3.3	3.2
Sr₂RuYO₆	2840.2	2843.1	2846.2	33.213	45.249	3.278	2.8	3.1
SrRuO₃	2839.2	2841.2	2843.9	20.964	29.95	12.38	2.9	2.8
CaRuO₃	2839.6	2841.9	2845.1	27.436	38.139	8.186	3.4	3.1

average of E_{B1} and E_{B2} (energies of peaks B1 and B2, respectively), *i.e.* $E_B = (E_{B1}I_{B1} + E_{B2}I_{B2})/(I_{B1} + I_{B2})$. The ΔE value of NH₄TcO₄ (2.5 eV) is less than that of SrTcO₃ (2.9 eV). This is to be expected because tetrahedral systems have less crystal-field-splitting ΔE (in the simplified crystal field theory $\Delta_{\text{Tet}} \sim 4/9\Delta_{\text{Oct}}$ assuming the same oxidation state and distances). This reduction is evident when comparing the spectra of the low (oct) and high (tet) temperature forms of Bi₂MoO₆ (3.1 *versus* 2.0 eV). The ΔE value also scales with the oxidation state of the cation. For example, ΔE for SrRu^{IV}O₃ (2.8 eV) is less than that of Sr₂Ru^{V}YO₆ (3.1 eV). In the present technetium oxides these two opposing factors result in a larger splitting in the octahedral Tc^{4+} oxide compared (2.9 eV) with the tetrahedral Tc^{7+} oxide (2.6 eV).

4. Conclusion

In conclusion, we have successfully demonstrated that the Tc *L*₃-edge can be measured by embedding a very small amount of technetium-containing powder samples (∼5 mg) in an epoxy resin. We have shown that the *L*-edge XANES spectra of the early 4*d* transition metals (Zr, Nb, Mo, Tc and Ru) are extremely sensitive to changes in both the oxidation state and coordination environment, providing information not only on the formal oxidation state of the cation but also on the crystal field splitting and coordination environment. Since the 4*d* orbitals are not fully occupied, the Tc *L*₃-edge spectrum directly probes the 4*d* bonding states, which can provide more accurate information on the local structure of Tc cations than the Tc *K*-edge spectrum. Crystal-field-splitting energies can be deduced from the Tc *L*₃-edge XANES spectra by fitting the spectra with component peaks. The methodology used here can easily be extended to other technetium species of various oxidation states and coordination environments, an important step in exploring this relatively unknown area of X-ray absorption spectroscopy.

Figure 6
Fitted Tc *L*₃-edge XANES spectra of (*a*) NH₄TcO₄ and (*b*) SrTcO₃.

corresponds to three unique peaks. By comparison, the first derivative Tc *L*₃-edge XANES spectrum of NH₄TcO₇ has only two peak maxima. In order to reduce the number of free parameters, peak widths were constrained so that all peaks in a spectrum had the same width. Crystal-field-splitting energy (ΔE) can be taken as the energy difference between peaks A and B. For octahedral systems, ΔE is taken as the energy difference between E_A (energy of peak A) and the weighted

References

Almahamid, I., Bryan, J. C., Bucher, J. J., Burrell, A. K., Edelstein, N. M., Hudson, E. A., Kaltsoyannis, N., Lukens, W. W., Shuh, D. K., Nitsche, H. & Reich, T. (1995). *Inorg. Chem.* **34**, 193–198.
Antonini, M., Caprile, C., Merlini, A., Petiau, J. & Thornley, F. R. (1983). *EXAFS and Near Edge Structure*, edited by A. Bianconi, L. Incoccia & S. Stipcich, pp. 261–264. Berlin/Heidelberg: Springer.
Avdeev, M., Thorogood, G. J., Carter, M. L., Kennedy, B. J., Ting, J., Singh, D. J. & Wallwork, K. S. (2011). *J. Am. Chem. Soc.* **133**, 1654–1657.
Bare, S. R., Mitchell, G. E., Maj, J. J., Vrieland, G. E. & Gland, J. L. (1993). *J. Phys. Chem.* **97**, 6048–6053.

Blanchard, P. E. R., Clements, R., Kennedy, B. J., Ling, C. D., Reynolds, E., Avdeev, M., Stampfl, A. P. J., Zhang, Z. M. & Jang, L. Y. (2012). *Inorg. Chem.* **51**, 13237–13244.

Blanchard, P. E. R., Liu, S., Kennedy, B. J., Ling, C. D., Avdeev, M., Aitken, J. B., Cowie, B. C. C. & Tadich, A. (2013*b*). *J. Phys. Chem. C*, **117**, 2266–2273.

Blanchard, P. E. R., Liu, S., Kennedy, B. J., Ling, C. D., Zhang, Z. M., Avdeev, M., Cowie, B. C. C., Thomsen, L. & Jang, L. Y. (2013*a*). *Dalton Trans.* **42**, 14875–14882.

Bréard, Y., Hardy, V., Raveau, B., Maignan, A., Lin, H. J., Jang, L. Y., Hsieh, H. H. & Chen, C. T. (2007). *J. Phys. Condes. Matter*, **19**, 216212.

Buttrey, D. J., Vogt, T., Wildgruber, U. & Robinson, W. R. (1994). *J. Solid State Chem.* **111**, 118–127.

Cowie, B. C. C., Tadich, A. & Thomsen, L. (2010). *AIP Conf. Proc.* **1234**, 307–310.

Dann, T.-E., Chung, S.-C., Huang, L.-J., Juang, J.-M., Chen, C.-I. & Tsang, K.-L. (1998). *J. Synchrotron Rad.* **5**, 664–666.

Deutsch, E., Libson, K., Jurisson, S. & Lindoy, L. F. (1983). *Prog. Inorg. Chem.* **30**, 75–139.

Fairley, N. (2012). *CasaXPS*, version 2.3.17dev5.9n. Casa Software Ltd, Teignmouth, Devon, UK.

Ferrier, M., Weck, P. F., Poineau, F., Kim, E., Stebbins, A., Ma, L. Z., Sattelberger, A. P. & Czerwinski, K. R. (2012). *Dalton Trans.* **41**, 6291–6298.

Glover, C., McKinlay, J., Clift, M., Barg, B., Boldeman, J., Ridgway, M., Foran, G., Garrett, R., Lay, P. & Broadbent, A. (2007). *AIP Conf. Proc.* **882**, 884–886.

Hartmann, T., Alaniz, A. J. & Antonio, D. J. (2012). *Proc. Chem.* **7**, 622–628.

Hartmann, T., Alaniz, A., Poineau, F., Weck, P. F., Valdez, J. A., Tang, M., Jarvinen, G. D., Czerwinski, K. R. & Sickafus, K. E. (2011). *J. Nucl. Mater.* **411**, 60–71.

Hu, H. C., Wachs, I. E. & Bare, S. R. (1995). *J. Phys. Chem.* **99**, 10897–10910.

Ikeno, H., Krause, M., Hoche, T., Patzig, C., Hu, Y. F., Gawronski, A., Tanaka, I. & Russel, C. (2013). *J. Phys. Condens. Matter*, **25**, 165505.

Kettle, S. F. A. (2008). *Symmetry and Structure: Readable Group Theory for Chemists.* New York: Wiley.

Kotegov, K. V., Pavlov, O. N. & Shvedov, V. P. (1968). *Advances in Inorganic Chemistry and Radiochemistry*, edited by H. J. Emeléus & A. G. Sharpe, pp. 1–90. New York: Academic Press.

Kozimor, S. A., Yang, P., Batista, E. R., Boland, K. S., Burns, C. J., Clark, D. L., Conradson, S. D., Martin, R. L., Wilkerson, M. P. & Wolfsberg, L. E. (2009). *J. Am. Chem. Soc.* **131**, 12125–12136.

Laarif, A., Theobald, F. R., Vivier, H. & Hewat, A. W. (1984). *Z. Kristallogr.* **167**, 117–124.

Lede, E. J., Requejo, F. G., Pawelec, B. & Fierro, J. L. G. (2002). *J. Phys. Chem. B*, **106**, 7824–7831.

Mausolf, E., Poineau, F., Droessler, J. & Czerwinski, K. R. (2011). *J. Radioanal. Nucl. Chem.* **288**, 723–728.

Middey, S., Nandy, A. K., Pandey, S. K., Mahadevan, P. & Sarma, D. D. (2012). *Phys. Rev. B*, **86**, 104406.

Mravlje, J., Aichhorn, M. & Georges, A. (2012). *Phys. Rev. Lett.* **108**, 197202.

Poineau, F., Sattelberger, A. P., Conradson, S. D. & Czerwinski, K. R. (2008). *Inorg. Chem.* **47**, 1991–1999.

Qasim, I., Kennedy, B. J., Zhang, Z. M., Avdeev, M. & Jang, L. Y. (2011). *J. Phys. Condens. Matter*, **23**, 435401.

Ravel, B. & Newville, M. (2005). *J. Synchrotron Rad.* **12**, 537–541.

Ray, S. C., Hsueh, H. C., Wu, C. H., Pao, C. W., Asokan, K., Liu, M. T., Tsai, H. M., Chuang, C. H., Pong, W. F., Chiou, J. W., Tsai, M. H., Lee, J. M., Jang, L. Y., Chen, J. M. & Lee, J. F. (2011). *Appl. Phys. Lett.* **99**, 042909.

Reynolds, E., Blanchard, P. E. R., Kennedy, B. J., Ling, C. D., Liu, S., Avdeev, M., Zhang, Z. M., Cuello, G. J., Tadich, A. & Jang, L. Y. (2013). *Inorg. Chem.* **52**, 8409–8415.

Ricciardo, R. A., Cuthbert, H. L., Woodward, P. M., Zhou, Q., Kennedy, B. J., Zhang, Z. M., Avdeev, M. & Jang, L. Y. (2010). *Chem. Mater.* **22**, 3369–3382.

Rodriguez, E. E., Poineau, F., Llobet, A., Kennedy, B. J., Avdeev, M., Thorogood, G. J., Carter, M. L., Seshadri, R., Singh, D. J. & Cheetham, A. K. (2011). *Phys. Rev. Lett.* **106**, 067201.

Sankar, G., Roberts, M. A., Thomas, J. M., Kulkarni, G. U., Rangavittal, N. & Rao, C. N. R. (1995). *J. Solid State Chem.* **119**, 210–215.

Schneller, T., Kohlstedt, H., Petraru, A., Waser, R., Guo, J., Denlinger, J., Learmonth, T., Glans, P. A. & Smith, K. E. (2008). *J. Sol-Gel Sci. Technol.* **48**, 239–252.

Thorogood, G. J., Avdeev, M., Carter, M. L., Kennedy, B. J., Ting, J. & Wallwork, K. S. (2011*a*). *Dalton Trans.* **40**, 7228–7233.

Thorogood, G. J., Zhang, Z. M., Hester, J. R., Kennedy, B. J., Ting, J., Glover, C. J. & Johannessen, B. (2011*b*). *Dalton Trans.* **40**, 10924–10926.

Ting, J., Kennedy, B. J., Zhang, Z., Avdeev, M., Johannessen, B. & Jang, L. Y. (2010). *Chem. Mater.* **22**, 1640–1646.

Veith, G. M., Greenblatt, M., Croft, M., Ramanujachary, K. V., Hattrick-Simpers, J., Lofland, S. E. & Nowik, I. (2005). *Chem. Mater.* **17**, 2562–2567.

Wu, H. H., Chen, S. W., Lin, B. N., Hsu, Y. Y., Lee, J. F., Jang, L. Y. & Ku, H. C. (2003). *J. Low Temp. Phys.* **131**, 1193–1197.

Yamamoto, T. (2008). *X-ray Spectrom.* **37**, 572–584.

Zhou, Q. D., Kennedy, B. J., Zhang, Z. M., Jang, L. Y. & Aitken, J. B. (2009). *Chem. Mater.* **21**, 4203–4209.